Sensors and Materials, Vol. 38, No. 10 (2026) 6227–6240
MYU Tokyo

S & M 4677

Conductivity Enhancement Study of Poly(vinyl alcohol)/Glycerol–Poly(3,4-ethylenedioxythiophene): Poly(styrenesulfonate)/Lignin/Cellulose Nanocrystal Sensors

Yu-Hsiang Chang, Guan-Yu Chen, and Shih-Chen Shi*

Department of Mechanical Engineering, National Cheng Kung University (NCKU),
No. 1, University Road, Tainan 70101, Taiwan

(Received June 30, 2026; accepted October 5, 2026)

Keywords: conductive hydrogels, strain sensors, dialdehyde cellulose nanocrystals, graphene quantum dots, PEDOT:PSS

With the rapid development of wearable technologies, the demand for high-performance strain sensors with excellent electrical conductivity has significantly increased. In this study, we aimed to enhance the electrical conductivity of a poly(vinyl alcohol)/glycerol–poly(3,4-ethylened ioxythiophene):poly(styrenesulfonate)/lignin/cellulose nanocrystal hydrogel sensor, which originally exhibited real-time human motion detection capabilities but showed inferior conductivity. A multi-stage green enhancement strategy was systematically investigated using various additives, including dimethyl sulfoxide (DMSO), dialdehyde cellulose nanocrystals (DACNCs), and graphene quantum dots (GQDs). First, the addition of DMSO promoted phase separation within the polymer matrix, increasing the initial conductivity from 1.73 to 5.36 S/m. Second, periodate oxidation was utilized to prepare DACNCs, and adding this functionalized nanomaterial further optimized the conductive network, elevating the conductivity to 9.75 S/m, which is 4.43 times that of the original film. Finally, the incorporation of GQDs acted as conductive nanobridges, successfully driving the overall electrical conductivity beyond the 20 S/m milestone. The resulting composite film effectively resolves the intrinsic conductivity limitations of traditional hydrogels, demonstrating immense potential for advanced wearable applications in medical healthcare, electrocardiogram monitoring, and artificial skin.

1. Introduction

The rapid development of wearable technology is profoundly reshaping the landscape of personalized healthcare.(1) For epidermal electronic devices designed for applications such as electrocardiography and continuous motion monitoring, the core materials must simultaneously exhibit high sensitivity, exceptional mechanical durability, long-lasting moisture retention, and excellent electrical conductivity.(2) Recent studies on flexible wearable motion sensors have further highlighted the importance of simultaneously optimizing electrical conductivity and strain-sensing characteristics to achieve accurate and stable motion detection.(3) Compared with

*Corresponding author: e-mail: scshi@mail.ncku.edu.tw
https://doi.org/10.18494/SAM6504

ISSN 0914-4935 © MYU K.K.
https://myukk.org/

traditional rigid electrodes, which are bulky and prone to signal degradation, flexible conductive hydrogels have emerged as a highly promising alternative owing to their tissue-like softness and seamless skin-interfacial integration.[4]

Among various conductive materials, the polymer poly(3,4-ethylenedioxythiophene): poly(styrenesulfonate) (PEDOT:PSS) exhibits excellent water processability and thermal stability; however, its intrinsic electrical conductivity remains insufficient to meet the stringent demands of high-performance biomedical applications.[5–7] Moreover, pure hydrogels are highly susceptible to rapid dehydration and mechanical failure under continuous strain.[8,9] To overcome these bottlenecks, in this study, we introduce polyvinyl alcohol and glycerol (GLY) to endow the material with superior flexibility and anti-dehydration capabilities.[10] Furthermore, biomass fillers such as lignin and cellulose nanocrystals (CNCs) are incorporated into the system to further stabilize the overall composite structure by constructing a robust skeletal network and facilitating intermolecular hydrogen bonding.[11,12] Furthermore, biomass fillers such as lignin and CNCs have been increasingly incorporated into flexible hydrogel and conductive polymer systems to improve mechanical stability and wearable sensing performance. For example, CNC-reinforced biomimetic poly(vinyl alcohol)/polyacrylic acid (PVA/PAA) hydrogels have demonstrated enhanced wearable sensor functionality, while the combined incorporation of CNCs and self-assembling lignin into PEDOT:PSS/PVA composites has been shown to improve mechanical and self-powered wearable properties.[13,14]

To further improve electrical conductivity, we introduce a sequential three-stage conductivity-enhancement strategy based on dimethyl sulfoxide (DMSO), dialdehyde cellulose nanocrystals (DACNCs), and graphene quantum dots (GQDs). In the first stage, DMSO is used to modify the molecular organization of PEDOT:PSS by promoting conformational rearrangement and phase separation between PEDOT- and PSS-rich regions, thereby improving the connectivity of conductive pathways.[15] Recent studies have also demonstrated that DMSO treatment is effective for enhancing the electrical performance of PEDOT:PSS-based hydrogels for flexible conductive sensor applications.[16] In the second stage, CNCs are functionalized through periodate oxidation to form DACNCs. The introduced aldehyde groups modify the interfacial interactions within the composite and assist the rearrangement of the PEDOT:PSS conductive network while retaining the structural contribution of the original CNC framework. In the third stage, GQDs are incorporated as nanoscale conductive bridges. Their graphitic domains can interact with PEDOT chains through π–π interactions, facilitating more ordered chain organization and improving charge transport between adjacent conductive regions.[17]

In this study, we propose a three-stage enhancement strategy to fabricate a high-performance PVA/Gly-PEDOT:PSS/lignin (LNM)/CNC/DACNC/GQD wearable sensor, aiming to resolve the intrinsic trade-off between electrical conductivity and mechanical flexibility. We hypothesize that DMSO initiates PEDOT:PSS phase separation, functionalized DACNCs further eliminate insulating PSS barriers while maintaining structural integrity, and GQDs bridge microscopic gaps to construct continuous charge transport pathways. By optimizing these modifiers, we aim to break the conductivity ceiling of traditional hydrogels (>20 S/m). The resulting composite film balances electrical, mechanical, and moisture-retaining properties, providing a robust platform for next-generation ECG and epidermal electronics.

2. Materials and Methods

2.1 Materials

PVA, CNC, GLY, LNM, PEDOT:PSS, and DMSO were used for the preparation of the sensor films. Sodium periodate ($NaIO_4$), ethylene glycol, hydrochloric acid (HCl), sodium hydroxide (NaOH), sulfuric acid (H_2SO_4), and phenolphthalein were used for the synthesis and titration of DACNC. Glucose was utilized as the precursor for synthesizing GQDs. Deionized (DI) water and reverse osmosis (RO) water were used throughout the experiments. All chemicals were used as received without further purification.

2.2 Preparation of PVA/Gly-PEDOT:PSS/LNM/CNC composite films

The composite sensor films were fabricated via a physical blending and freeze-thaw method. Initially, 22.2 g of PVA powder and 11 g of glycerol were added to 200 mL of DI water and heated at 90 ℃ in an oven for 1.5 to 2 h until complete dissolution, followed by cooling to room temperature. Concurrently, 3 g of CNC powder was uniformly dispersed in 100 mL of DI water under magnetic stirring for 2 h. To prepare the conductive additive, 3 mg of LNM was dissolved in varying volumes of DMSO (3, 5, 7, 9, and 11 mL) and ultrasonicated for 20 min. This LNM/DMSO mixture was then added to 5 mL of PEDOT:PSS solution and ultrasonicated for an additional 20 min to form the LNM/PEDOT:PSS suspension. Subsequently, 10 mL of the CNC dispersion and the LNM/PEDOT:PSS suspension were sequentially added into the PVA/glycerol solution. The final mixture was magnetically stirred for 2 h to ensure homogeneous dispersion. The blend was then poured into a mold and subjected to three consecutive freeze-thaw cycles (freezing at −20 ℃ for 2 h and thawing at room temperature for 1 h) to induce physical crosslinking, yielding a transparent and uniform composite film. The detailed experimental parameters for samples with varying DMSO volumes are summarized in Table 1.

2.3 Synthesis of DACNC and GQDs

DACNC was synthesized via the selective periodate oxidation of CNCs. The pH of a CNC aqueous suspension was adjusted to 4.5 using diluted HCl, and the mixture was heated to 45 ℃.

Table 1
Experimental parameters for the preparation of composite films with varying DMSO volumes.

Sample/ experiment	PVA (g)	GLY (g)	CNC (g)	PEDOT:PSS (mL)	LNM (mg)	DMSO (mL)
DMSO_3	22.2	11	3	5	3	3
DMSO_5	22.2	11	3	5	3	5
DMSO_7	22.2	11	3	5	3	7
DMSO_9	22.2	11	3	5	3	9
DMSO_11	22.2	11	3	5	3	11

Next, 6 g of $NaIO_4$ was added, and the reaction vessel was wrapped in aluminum foil to prevent light-induced decomposition. The oxidation reaction was carried out at 45 °C under continuous stirring at 240 rpm for 12 h. After the reaction, 15 mL of ethylene glycol was added to quench the unreacted $NaIO_4$. The resulting mixture was dialyzed against RO water for 2 to 3 days to remove residual salts, followed by freeze-drying (FD-1A-50, Boyikang) for 1 to 2 days to obtain solid DACNC powder. The experimental parameters for fabricating DACNC-modified composite films are summarized in Table 2.

GQDs were prepared using a bottom-up hydrothermal approach. Briefly, 70 mg of glucose was dissolved in 70 mL of DI water and stirred thoroughly. The solution was transferred into a Teflon-lined autoclave, purged with argon gas to eliminate internal air, and sealed tightly. The hydrothermal reaction was conducted at a target internal temperature of 200 °C for 2 h. After cooling, the resulting liquid was filtered through a 0.22 μm microporous membrane and centrifuged at 15000 rpm for 30 min to separate large unreacted particles and graphene oxide. The supernatant was then dialyzed for 24 h to obtain the highly purified GQD solution. The experimental parameters for fabricating GQD-doped composite films are presented in Table 3.

2.4 Characterization methods

The chemical structures and functional-group transformations of pristine CNCs and synthesized DACNCs were characterized by Fourier-transform infrared spectroscopy (FTIR, Thermo Nicolet iS5, USA) equipped with an iD1 transmission accessory over a wavenumber range of 4000–500 cm^{-1}. To evaluate the degree of cellulose oxidation, the aldehyde-group content of DACNCs (W, μmol/g) was quantified using an acid–base back-titration method. Briefly, 0.2 g of DACNCs was reacted with 0.2 M NaOH at 70 °C for 2 min, followed by the addition of 0.2 M H_2SO_4. The remaining acid was subsequently back-titrated with 0.2 M NaOH using phenolphthalein as the indicator.

Table 2
Experimental parameters for DACNC-modified composite films.

Sample/ experiment	PVA (g)	GLY (g)	CNC (g)	PEDOT:PSS (mL)	LNM (mg)	DMSO (mL)	DACNC (g)
DACNC_0	22.2	11	3	5	3	5	0
DACNC_1	22.2	11	3	5	3	5	1
DACNC_3	22.2	11	3	5	3	5	3
DACNC_5	22.2	11	3	5	3	5	5

Table 3
Experimental parameters for GQD-doped composite films.

Sample/ experiment	PVA (g)	GLY(g)	CNC (g)	PEDOT:PSS (mL)	LNM (mg)	DMSO (mL)	PVA (g)	GQD (mL)
GQD_5	22.2	11	3	5	3	5	1	0.25
GQD_10	22.2	11	3	5	3	5	1	0.5
GQD_15	22.2	11	3	5	3	5	1	0.75

The electrical properties of the PVA/Gly-PEDOT:PSS/LNM/CNC composite films, including Hall-derived carrier mobility, resistivity, and bulk carrier concentration, were evaluated at room temperature using a Hall-effect measurement system with a four-point probe configuration (National Kaohsiung University of Science and Technology, Taiwan). Each sample was measured ten times under identical measurement conditions, and the reported electrical properties represent the averages of these repeated measurements. Because complete individual replicate data were not retained for all samples, reliable statistical dispersion parameters, such as standard deviation, could not be retrospectively calculated and are therefore not reported in the present study. Electrical conductivity was subsequently determined from the measured resistivity. Because the investigated films consist of heterogeneous polymeric, cellulose-based, and conductive phases, the Hall-derived mobility is interpreted as an apparent or effective Hall mobility representing the overall charge-transport response of the composite conductive network, rather than the intrinsic band mobility of PEDOT:PSS.

Finally, the mechanical properties of the composite films were evaluated by tensile testing using a universal testing machine at a constant crosshead speed of 10 mm/min. The measured load and displacement data were converted into engineering stress (σ) and engineering strain (ε) to obtain the corresponding stress–strain curves.

3. Results and Discussion

3.1 Effect of DMSO on conductivity

The electrical properties of PVA/Gly-PEDOT:PSS/LNM/CNC sensor films containing different amounts of DMSO (3–11 mL) were evaluated using a Hall-effect measurement system. As shown in Figs. 1(b) and 1(c), increasing the DMSO content progressively decreased the measured resistivity from 0.73 to 0.19 Ω·cm, accompanied by an increase in electrical conductivity from 1.38 to 5.36 S/m.

The conductivity enhancement is attributed to the effect of DMSO on the molecular organization of PEDOT:PSS. The highly polar DMSO interacts strongly with the PSS chains, promoting partial phase separation between PEDOT- and PSS-rich regions and improving the connectivity of conductive domains. Moreover, DMSO can induce a conformational rearrangement of PEDOT chains toward a more extended structure, which facilitates charge transport between adjacent PEDOT-rich regions. Consistent with these structural changes, the measured bulk carrier concentration increased from 3.17×10^{16} to 2.23×10^{17} cm^{-3} as the DMSO content increased.

The Hall-derived mobility also increased markedly with DMSO addition, from 558.47 $cm^2/V{\cdot}s$ at 3 mL to 27380 $cm^2/V{\cdot}s$ at 11 mL, as shown in Fig. 1(a). Because the present material is a heterogeneous multiphase composite rather than a homogeneous semiconductor, these unusually high values should not be interpreted as the intrinsic carrier mobility of PEDOT:PSS. Instead, they are more appropriately regarded as the apparent or effective Hall mobility reflecting changes in the overall connectivity and charge-transport behavior of the composite conductive network. Therefore, the increasing Hall-derived mobility, together with the decrease in resistivity, indicates improved effective charge transport following DMSO treatment.

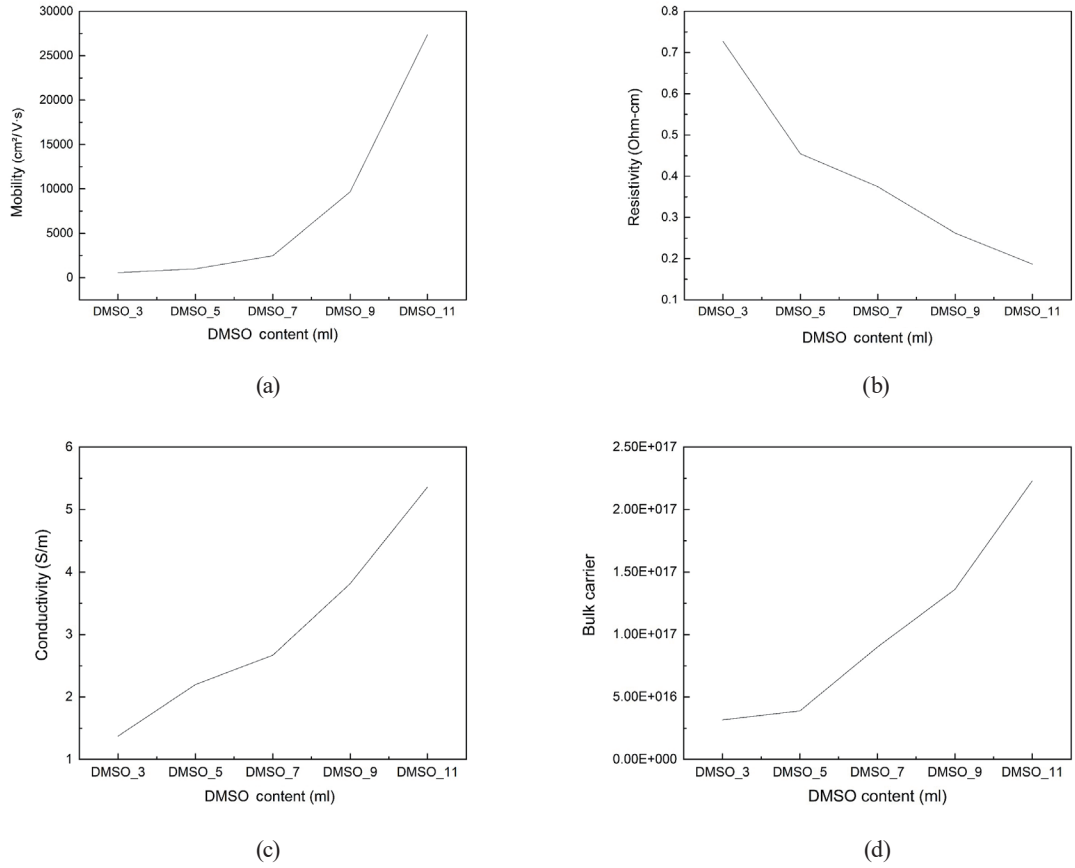


Fig. 1. Electrical properties of composite films as a function of DMSO content: (a) carrier mobility, (b) resistivity, (c) electrical conductivity, and (d) bulk carrier concentration.

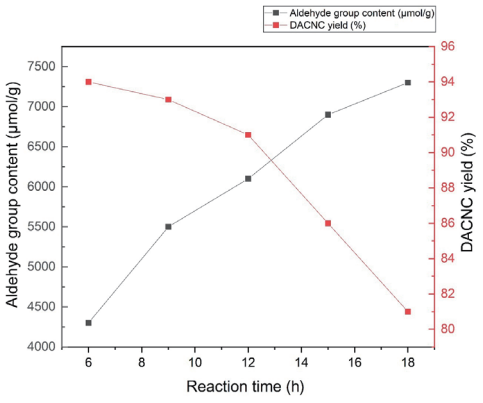
Although 11 mL of DMSO produced the highest electrical conductivity among the investigated formulations, excessive DMSO may adversely affect the cellulose-containing network by promoting CNC swelling and weakening the PVA–CNC intermolecular interactions, thereby reducing mechanical stability. Therefore, 5 mL of DMSO, corresponding to a conductivity of 2.20 S/m, was selected as the baseline formulation for the subsequent DACNC and GQD modification experiments to maintain a more appropriate balance between electrical enhancement and structural integrity.

3.2 Chemical structure and optimization of DACNCs

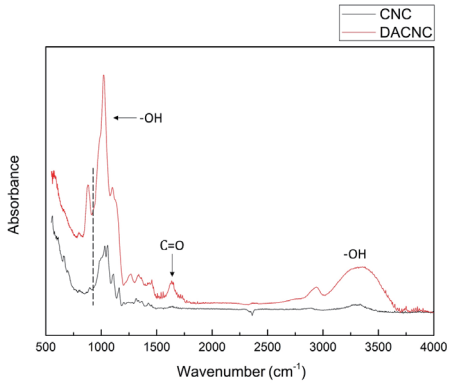
DACNCs, exhibiting a white, porous sponge-like appearance after freeze-drying [Fig. 2(a)], were synthesized via selective periodate oxidation. To balance the degree of oxidation and production efficiency, the reaction time was systematically optimized. As shown in Fig. 2(b), the aldehyde group content steadily increased while the production yield decreased over time. A 12 h reaction time was determined to be optimal, achieving a high aldehyde content of



(a)



(b)



(c)

Fig. 2. (Color online) Characterization and optimization of DACNCs: (a) Optical image of freeze-dried DACNCs, (b) effects of reaction time on aldehyde group content and production yield, and (c) comparative FTIR spectra of pristine CNCs and synthesized DACNCs.

approximately 6100 μmol/g alongside an excellent yield of 91%. This specifically optimized formulation was adopted for all subsequent sensor modifications.

The successful structural modification of the cellulose was confirmed by FTIR spectroscopy [Fig. 2(c)]. While both the pristine CNCs and DACNCs retained the characteristic cellulose backbone absorption peaks near 1000 cm^{-1}, the DACNC spectrum exhibited a notable red-shift due to hemiacetal formation. Most importantly, a distinct new absorption peak emerged in the 1500–1700 cm^{-1} range for the DACNC sample, corresponding to the stretching vibrations of the newly formed aldehyde (C=O) groups. Concurrently, the intensity of the broad hydroxyl (–OH) band between 3000 and 4000 cm^{-1} significantly decreased. These spectral changes provide concrete evidence that a substantial portion of the original hydroxyl groups on the CNCs was successfully converted into aldehyde groups.

3.3 Mechanical and electrical performance of DACNC-modified sensors

To evaluate the structural effect of DACNCs, pristine CNCs were completely replaced with DACNCs in the formulation containing 5 mL of DMSO. As shown in Fig. 3(a), this substitution decreased the tensile stress from 65.9 to 60 MPa and the elongation at break from 320 to 250%. The decline in mechanical performance is attributed to the structural changes induced by periodate oxidation. During oxidation, the cleavage of the C2–C3 bonds partially disrupts the original crystalline structure of CNCs, thereby reducing its effectiveness as a rigid reinforcing phase within the PVA matrix. Consequently, complete replacement with DACNCs weakens the structural reinforcement originally provided by pristine CNCs and results in lower tensile strength and ductility.

Despite this mechanical trade-off, DACNC substitution improved the electrical properties of the composite films, as shown in Figs. 3(b)–3(e). The Hall-derived mobility increased to 3200 $cm^2/V{\cdot}s$, while the bulk carrier concentration reached 1.01×10^{17} cm^{-3}. Moreover, the resistivity decreased to 0.34 Ω·cm and the conductivity increased from 2.20 to 2.98 S/m. This electrical enhancement may be associated with the aldehyde-functionalized surface of DACNCs, which modifies the interfacial interactions within the PEDOT:PSS-containing network and promotes the reorganization of conductive domains. Previous studies have reported that modifying the interactions between PEDOT and PSS can facilitate phase separation and improve the connectivity of PEDOT-rich conductive regions.[18] Such structural rearrangement can facilitate charge transport through the composite network. However, the simultaneous loss of the rigid CNC framework indicates that complete DACNC substitution improves electrical transport at the expense of mechanical reinforcement, motivating the subsequent strategy of retaining pristine CNCs while directly adding DACNCs.

3.4 Effects of DACNC addition on electrical properties

To overcome the mechanical deterioration observed after complete CNC substitution, DACNCs were directly added at 1, 3, and 5 g while retaining 3 g of pristine CNCs in the baseline formulation containing 5 mL of DMSO. This approach was designed to preserve the rigid reinforcing framework provided by CNCs while introducing the functional groups of DACNCs to further regulate the conductive network. As shown in Figs. 4(a)–4(d), increasing the DACNC content progressively improved the electrical properties of the composite films. At 5 g of DACNCs, the Hall-derived mobility increased to 31630 $cm^2/V{\cdot}s$, while the bulk carrier concentration reached 3.02×10^{17} cm^{-3}. On the other hand, the resistivity decreased from 0.45 to 0.10 Ω·cm, while the electrical conductivity increased from 2.20 to 9.75 S/m, corresponding to a 4.43-fold enhancement.

Because the composite film consists of multiple polymeric, cellulose-based, and conductive phases, the unusually high Hall-derived mobility should not be interpreted as the intrinsic carrier mobility of PEDOT:PSS. Instead, it is more appropriately regarded as an apparent or effective Hall mobility reflecting the overall charge-transport behavior of the heterogeneous

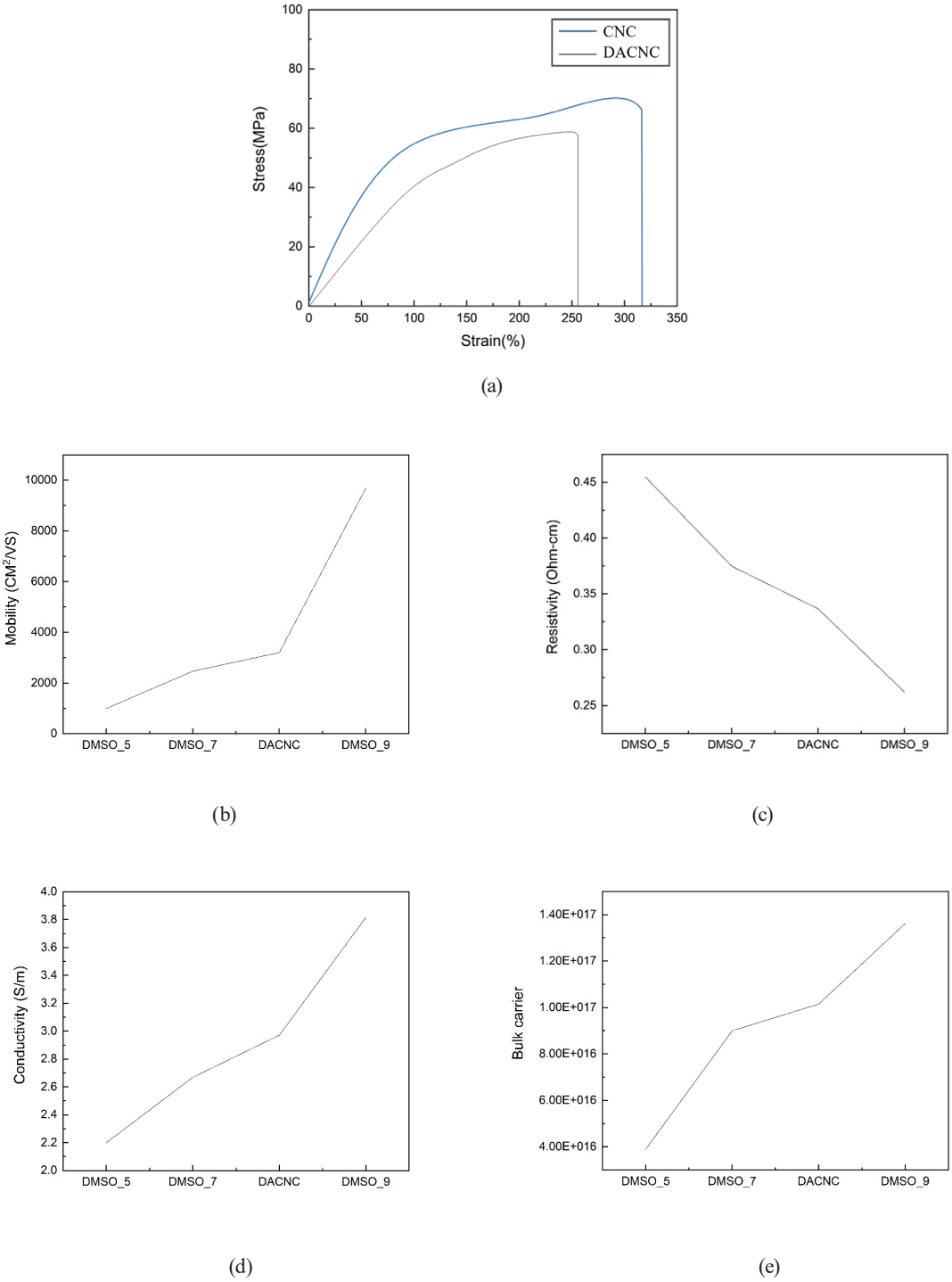


Fig. 3. (Color online) Mechanical and electrical performance comparison of sensors modified by DACNC substitution: (a) stress-strain curves, (b) carrier mobility, (c) resistivity, (d) electrical conductivity, and (e) bulk carrier concentration.

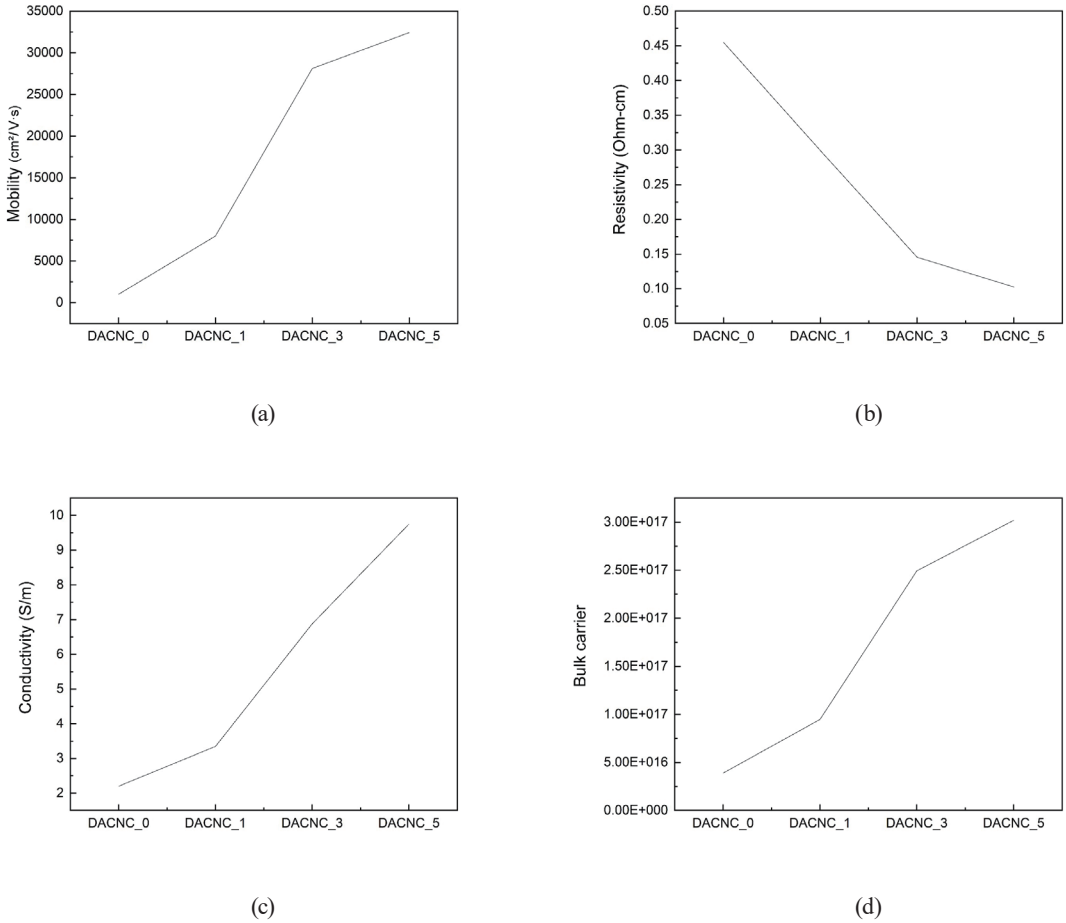


Fig. 4. Electrical properties of composite films with various DACNC contents: (a) carrier mobility, (b) resistivity, (c) electrical conductivity, and (d) bulk carrier concentration.

conductive network. The simultaneous increases in Hall-derived mobility and carrier concentration suggest that DACNCs modify the interfacial environment and improve the connectivity of PEDOT-rich conductive regions, thereby facilitating effective charge transport throughout the composite film.

Compared with complete CNC substitution, direct DACNC addition provides a more favorable balance between mechanical reinforcement and electrical enhancement. The retained pristine CNCs continue to serve as a rigid structural framework, whereas the added DACNCs contribute additional interfacial interactions and assist the reorganization of PEDOT:PSS conductive domains. These complementary roles promote the formation of more continuous charge-transport pathways while avoiding the substantial loss of mechanical reinforcement associated with complete CNC replacement. Therefore, retaining CNCs while introducing DACNCs represents a more effective strategy for improving the electrical performance of the composite sensor without unnecessarily sacrificing its structural integrity.

3.5 Conductivity enhancement via GQD integration

To further enhance the electrical performance of the DACNC-modified sensor films, GQDs were introduced as functional nanofillers. The GQDs were incorporated into the PVA/Gly-PEDOT:PSS/LNM/CNC/DACNC matrix at PEDOT:PSS/GQD mass ratios of 100:5, 100:10, and 100:15. As shown in Fig. 5, the electrical conductivity increased progressively with increasing GQD content, from 8.82 S/m at 100:5 to 14.07 S/m at 100:10 and 20.88 S/m at 100:15.

The conductivity enhancement can be associated with the π-conjugated structure of GQDs and their interfacial interactions with PEDOT:PSS. The graphitic domains of GQDs contain delocalized π electrons that can interact noncovalently with the conjugated PEDOT backbone through π–π interactions. These interactions promote the closer interfacial contact and more favorable organization of PEDOT chains around the GQD surface. In this manner, GQDs can act as nanoscale bridges between neighboring PEDOT-rich conductive domains, providing additional connections across regions that would otherwise be separated by relatively less-conductive polymer- or PSS-rich domains.

The formation of these nanoscale connections improves the continuity of the conductive network and may reduce the effective barrier for charge hopping between adjacent PEDOT-rich regions. In addition, hydrophilic interactions between the surface functional groups of GQDs and PSS may promote the redistribution of the PSS-rich phase, thereby further facilitating interfacial charge transport. Therefore, the GQD-induced conductivity enhancement is attributed to the combined effects of π–π-assisted PEDOT chain

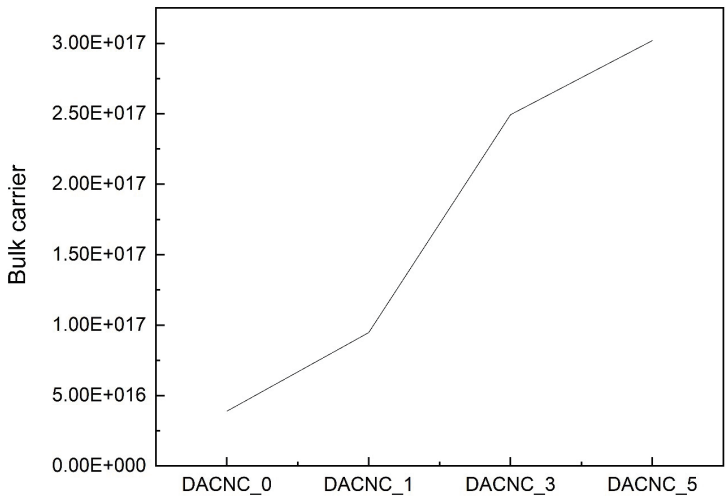


Fig. 5. Electrical conductivity of composite films as a function of GQD content (PEDOT:PSS/GQD mass ratios of 100:5, 100:10, and 100:15).

organization, the nanoscale bridging of conductive domains, and improved PEDOT/PSS interfacial organization. Together with the DACNC-regulated conductive network, these effects provide more continuous charge-transport pathways throughout the composite matrix.[19] Consequently, the conductivity reached 20.88 S/m at the highest investigated GQD content, demonstrating the effectiveness of the sequential multi-level conductivity-enhancement strategy.

To further contextualize the electrical performance of the present composite, the obtained conductivity was compared with recently reported conductive hydrogels for wearable sensing. Zheng *et al.* reported a silk fibroin/PVA hydrogel containing MXene, PEDOT:PSS, and reduced graphene oxide with an electrical conductivity of 6.67 S/m and an elongation of 315%.[20] Zhao *et al.* developed a PEDOT:PSS-based PPGP hydrogel exhibiting a conductivity of 3.4 S/m and a gauge factor of 10.63 for wearable strain sensing.[21] More recently, Luo *et al.* have reported a PVA/PAM/EG/PEDOT hydrogel with a conductivity of 32.39 S/m, a gauge factor of 2.17, a strain range of 0–1050%, and a response time of 95 ms.[22] In comparison, the maximum conductivity of 20.88 S/m obtained in the present study is higher than those of the MPRS and PPGP systems but lower than that of the PVA/PAM/EG/PEDOT hydrogel. The main distinction of the present work is the sequential DMSO/DACNC/GQD modification strategy for progressively regulating molecular organization, interfacial interactions, and nanoscale conductive bridging. Nevertheless, comprehensive gauge-factor, mechanical durability, response-time, and long-term cycling evaluations of the final GQD-containing formulation remain necessary for a more complete assessment of its wearable sensing performance.

4. Conclusions

In this study, the electrical conductivity of the PVA/Gly-PEDOT:PSS/LNM/CNC sensor film was significantly enhanced through the strategic incorporation of organic solvents, DACNCs, and GQDs. Initially, the introduction of DMSO effectively improved the conductivity of PEDOT:PSS. By incrementally increasing the DMSO content from 3 to 11 mL, the electrical performance exhibited a steady upward trend. Specifically, at an optimal addition of 11 mL, the conductivity reached 5.36 S/m, representing a 3.1-fold increase compared with the pristine film's baseline of 1.73 ± 0.99 S/m.

To further augment the film's properties, DACNCs featuring highly reactive aldehyde groups were successfully synthesized via the periodate oxidation of nanocellulose. The optimal reaction time was determined to be 12 h, yielding an ideal balance between the degree of oxidation and production efficiency by achieving an aldehyde group content of approximately 6100 μmole/g with an excellent yield of 91%. Subsequent experiments explored the trade-offs between substituting and adding DACNCs. Replacing 3 g of CNCs with 3 g of DACNCs in a film containing 5 mL of DMSO increased the conductivity to 2.98 S/m, achieving a 1.4-fold enhancement. However, this substitution compromised the mechanical integrity by reducing the tensile stress to 60 MPa and the maximum strain to 250%. Because such mechanical degradation can limit the sensor's operational lifespan, utilizing DACNCs as an additive rather than a substitute proved to be a superior strategy. Adding 1, 3, and 5 g of DACNCs to the original

formulation systematically increased the conductivity to 3.35, 6.88, and 9.75 S/m, respectively, with the 5 g addition pushing the performance close to the 10 S/m milestone.

Ultimately, to push the electrical performance even further, GQDs were introduced into the DACNC-enhanced composite film. By systematically adjusting the PEDOT:PSS to GQD mass ratio across 100:5, 100:10, and 100:15, it was demonstrated that higher GQD concentrations corresponded to remarkable improvements, successfully achieving an outstanding conductivity exceeding 20 S/m. In summary, the synergistic effects of optimized DMSO doping, DACNC addition, and GQD incorporation effectively overcame the conductivity limitations of the original composite, paving the way for the development of high-performance and highly durable wearable sensing devices.

Acknowledgments

This work was supported by the National Science and Technology Council (NSTC), Taiwan, under Grant Nos. 112-2221-E-006-173, 113-2221-E-006-087-MY2, 113-2221-E-006-112-MY2, and 113-2221-E-006-116. The authors gratefully acknowledge the Core Facility Center at National Cheng Kung University, Taiwan, for providing access to the EM000800 and SQUID000200 instruments, which were funded by the NSTC project 114-2740-M-006-001. Additional support from the Higher Education Sprout Project of the Ministry of Education, Taiwan, through the Headquarters of University Advancement at National Cheng Kung University (NCKU), is also gratefully acknowledged.

References

1 K. Brophy, S. Davies, S. Olenik, Y. Çotur, D. Ming, N. Van Zalk, D. O'Hare, F. Guder, and A. K. Yetisen: Imperial College London: London, UK (2021). https://doi.org/10.25561/88893
2 J. Ji, T. Su, J. Lu, X. Gao, and L. Zhang: BME Horizon **3** (2025) 202510. https://doi.org/10.70401/bmeh.2025.0004
3 Y.-K. Huang, S.-C. Shi, D. Rahmadiawan, and G.-Y. Chen: ACS omega **11** (2026) 4523. https://doi.org/10.1021/acsomega.5c10697
4 H. Yuk, B. Lu, and X. Zhao: Chem. Soc. Rev. **48** (2019) 1642. https://doi.org/10.1039/c8cs00595h
5 X. Crispin, F. Jakobsson, A. Crispin, P. Grim, P. Andersson, A. Volodin, C. Van Haesendonck, M. Van der Auweraer, W. R. Salaneck, and M. Berggren: Chem. Mater. **18** (2006) 4354. https://doi.org/10.1021/cm061032+
6 W. Li, Y. Li, Z. Song, Y.-X. Wang, and W. Hu: Chem. Soc. Rev. **53** (2024) 10575. https://doi.org/10.1039/d4cs00541d
7 S. Doshi, M. O. Forner, P. Wang, S. E. Hadwe, A. T. Jin, G. Dijk, K. Brinson, J. Lim, A. Dominguez-Alfaro, and C. Y. J. Lim: Adv. Mater. **37** (2025) 2415827. https://doi.org/10.1002/adma.202415827
8 C. Miao, P. Li, J. Yu, X. Xu, F. Zhang, and G. Tong: Gels **9** (2023) 224. https://doi.org/10.3390/gels9030224
9 X. Li and J. P. Gong: Nat. Rev. Mater. **9** (2024) 380. https://doi.org/10.1038/s41578-024-00672-3
10 Y. Zhong, Q. Lin, H. Yu, L. Shao, X. Cui, Q. Pang, Y. Zhu, and R. Hou: Front. Chem. **12** (2024) 1376799. https://doi.org/10.3389/fchem.2024.1376799
11 M. N. May, A. Sugawara, T.-A. Asoh, Y. Takashima, A. Harada, and H. Uyama: Polymer **277** (2023) 125979. https://doi.org/10.1016/j.polymer.2023.125979
12 Y. Wang, S. Liu, Q. Wang, X. Fu, and P. Fatehi: Cellulose **27** (2020) 8725. https://doi.org/10.1007/s10570-020-03396-z
13 S.-C. Shi, S.-T. Cheng, and D. Rahmadiawan: Sens. Actuators, A **379** (2024) 115981. https://doi.org/10.1016/j.sna.2024.115981
14 S.-C. Shi, Y.-C. Hsieh, and D. Rahmadiawan: ACS Omega **10** (2025) 14666. https://doi.org/10.1021/acsomega.4c07933

15 N. A. A. Shahrim, Z. Ahmad, A. W. Azman, Y. F. Buys, and N. Sarifuddin: Mater. Adv. **2** (2021) 7118. https://doi.org/10.1039/D1MA00690A
16 Y.-K. Huang, S.-C. Shi, G.-Y. Chen, and D. Rahmadiawan: Sens. Mater. **37** (2025) 4427. https://doi.org/10.18494/SAM5641
17 F. Sols, F. Guinea, and A. C. Neto: Phys. Rev. Lett. **99** (2007) 166803. https://doi.org/10.1103/PhysRevLett.99.166803
18 M. Donoval, M. Micjan, M. Novota, J. Nevrela, S. Kovacova, M. Pavuk, P. Juhasz, M. Jagelka, J. Kovac Jr., and J. Jakabovic: Appl. Surf. Sci. **395** (2017) 86. https://doi.org/10.1016/j.apsusc.2016.05.076
19 J. H. Song, J. Jeong, J. Park, G. Park, I. Imae, and J. Kwak: ACS Appl. Electron. Mater. **6** (2024) 6313. https://doi.org/10.1021/acsaelm.4c01357
20 Z. Zheng, W. Xu, Y. Wang, W. Xiong, C. Xiong, L. You, and S. Wang: Mater. Today Commun. **38** (2024) 108465. https://doi.org/10.1016/j.mtcomm.2024.108465
21 R. Zhao, X. Yan, H. Lin, Z. Zhao, and S. Song: Chem. Eng. J. **510** (2025) 161645. https://doi.org/10.1016/j.cej.2025.161645
22 R. Luo, K. Zhang, H. Li, Y. Cui, J. Hu, X. Zhou, W. Wang, and L. Li: Appl. Mater. Today **45** (2025) 102798. https://doi.org/10.1016/j.apmt.2025.102798